Quantum Stark broadening data for Ar viii and Ar ix lines

Rihab Aloui, Haykel Elabidi, Rafik Hamdi, Sylvie Sahal-Bréchot

Monthly Notices
of the
ROYAL ASTRONOMICAL SOCIETY

MNRAS **484,** 4801–4810 (2019)
Advance Access publication 2019 February 4

doi:10.1093/mnras/stz303

Quantum Stark broadening data for Ar VIII and Ar IX lines

Rihab Aloui,[1] Haykel Elabidi ,[2,3]★ Rafik Hamdi[2] and Sylvie Sahal-Bréchot[4]

[1]*Laboratoire de Spectroscopie et Dynamique Moléculaire, École Nationale Supérieure d'Ingénieurs de Tunis, University of Tunis, GRePAA, Tunis, Tunisia*
[2]*Department of Physics, Deanship of the Joint First Year, Umm Al-Qura University, Makkah Almukarramah, Saudi Arabia*
[3]*Laboratoire de Spectroscopie et Dynamique Moléculaire, Faculté des Sciences de Bizerte, University of Carthage, GRePAA, 7021, Zarzouna, Tunisia*
[4]*Observatoire de Paris, Sorbonne Université, Université PSL, CNRS, LERMA, F-92190 Meudon, France*

Accepted 2018 December 21. Received 2018 November 29; in original form 2018 November 10

ABSTRACT

We present in this paper quantum Stark broadening data for 14 Ar VIII and 16 Ar IX lines. For the Ar VIII ion, we compare our results to those calculated using the semiclassical method and we find an acceptable agreement. We performed also a comparison between the importance of Stark and Doppler broadening in the atmospheric conditions of DO white dwarfs. To the best of our knowledge, the Stark widths provided for the Ar IX ion are new, and no results have been found in the literature to compare with. We present some of the atomic radiative data used in our broadening calculations, and we compare them to other results. The comparison shows an acceptable agreement. Our results come to fill the lack of line broadening data necessary in stellar spectroscopy and plasma analysis.

Key words: atomic data – line: profiles – scattering – stars: atmospheres – white dwarfs.

1 INTRODUCTION

Knowledge of the atomic and line broadening data for many ions is needed in astrophysics, plasma physics, atmospheric physics, laser physics, and fusion research. Especially, Stark broadening process plays an important role in stellar spectroscopy; in particular, in astrophysical and laboratory plasmas analysis, they can be used for the determination of electron densities of laboratory plasmas, estimation of radiative transfer through the stellar plasmas, and for the determination of chemical abundances of elements (Dimitrijević 2003). The development of instruments and space astronomy stimulated the calculations of line broadening of trace elements in the X-ray wavelength range, for example, the new X-ray space telescope *Chandra*. Barstow, Hubeny & Holberg (1998) have shown that Stark broadening is dominant compared to the thermal Doppler one in white dwarf atmospheres, where their analysis needs models taking into account heavy element opacity. The lack of these data causes inaccuracy in the element abundance determination as noted in Rauch et al. (2007). Even though when line broadening data exist but not for required temperatures, the problem of abundance determination persists. In fact, in this case, we have to extrapolate the line widths to the required temperatures and densities. The accuracy of the extrapolation procedure is not always good and it can vary from ion to ion or from line to line. Consequently, calculations and production of line broadening data at required electron temperatures and densities is very useful for astrophysical and laboratory problems.

The recent finding of the far-UV lines of Ar VII (such as the line at 1063.55 Å) in the spectra of very hot central stars of planetary nebulae and white dwarfs (Werner, Rauch & Kruk 2007) confirmed the astrophysical interest for atomic and line broadening data for this element in diverse ionization stages. Argon is important in astrophysics and in fusion (Munoz Burgos et al. 2009; Ludlow et al. 2010), it is used as a carrier gas in plasma which contains mixture of other gases. Furthermore, Stark line widths of some Argon ions are missing in the literature, such as those of Ar IX. The present work is an effort to provide Stark broadening data for ions Ar VIII and Ar IX of astrophysical interests. The quantum mechanical method (Elabidi, Ben Nessib & Sahal-Bréchot 2004; Elabidi et al. 2008) has been used. The parameters used in our line broadening formula are evaluated during the calculation. This is done using the sequence of the UCL atomic codes SUPERSTRUCTURE (SST) (Eissner, Jones & Nussbaumer 1974), DISTORTED WAVE (DW) (Eissner 1998), and JAJOM (Saraph 1978) which have been recently adapted (Elabidi et al. 2008) to provide line broadening data besides the atomic and collision ones. These codes have been used for many years to provide only atomic radiative and collisional data. This attempt has been performed before for the Ar VII ion (Aloui et al. 2018), for Ar V and Ar VI ions (Elabidi & Sahal-Bréchot 2018), and for other ions in many works (Elabidi et al. 2008; Elabidi & Sahal-Bréchot 2011; Elabidi et al. 2011; Elabidi, Sahal-Bréchot & Dimitrijević 2014).Important results have been found, and acceptable agreements between our results and experimental/theoretical ones have been reported.

★ E-mail: haykel.elabidi@fsb.rnu.tn

Table 1. Present fine structure energy levels E in cm^{-1} for the Ar VIII ion compared to those of NIST database (Kramida et al. 2018) and to the Multiconfiguration Hartree–Fock (MCHF) results of Froese Fischer et al. (2006) with their relative errors in per cent.

i	Level	E	NIST	MCHF	Δ_{NIST}	Δ_{MCHF}
1	$3s\ ^2S_{1/2}$	0.0	0.0	0.0	–	–
2	$3p\ ^2P^o_{1/2}$	139667.	140095.	140354.56	0.31	0.49
3	$3p\ ^2P^o_{3/2}$	142312.	142808.2	143155.47	0.35	0.59
4	$3d\ ^2D_{3/2}$	332353.	332609.	334155.28	0.08	0.54
5	$3d\ ^2D_{5/2}$	332576.	332754.	334322.56	0.05	0.53
6	$4s\ ^2S_{1/2}$	573722.	575958.	577405.01	0.39	0.64
7	$4p\ ^2P^o_{1/2}$	625592.	628241.	629791.40	0.42	0.67
8	$4p\ ^2P^o_{3/2}$	626616.	629243.	630840.80	0.42	0.67
9	$4d\ ^2D_{3/2}$	694775.	697532.	699452.63	0.40	0.67
10	$4d\ ^2D_{5/2}$	694876.	697621.	699547.38	0.40	0.67

Our Stark broadening results for the Ar VIII ion have been compared to those obtained using the semiclassical approach (Dimitrijević & Sahal-Bréchot 1999), but to the best of our knowledge, there are no other results in the literature to perform comparisons for the ion Ar IX. The atomic radiative data used in our broadening calculations have been also compared to many other results such as the Multiconfiguration Dirac–Hartree–Fock (Froese Fischer, Tachiev & Irimia 2006) ones, the results from AUTOSTRUCTURE code (Zhou et al. 2015), and the CI relativistic calculations (Jönsson et al. 2014).

2 THEORY AND COMPUTATIONAL PROCEDURE

We present an outline of the quantum formalism of electron impact broadening. More details have been given elsewhere (Elabidi, Ben Nessib & Sahal-Bréchot (2004); Elabidi et al. (2008)). The calculations are performed within the frame of the impact approximation. This means that the time interval between collisions is much longer than the duration of a collision. The expression of the full width at half-maximum W expressed in angular frequency units obtained in Elabidi et al. (2008) is:

$$W = 2N_e \left(\frac{\hbar}{m}\right)^2 \left(\frac{2m\pi}{k_B T}\right)^{\frac{1}{2}} \int_0^\infty \Gamma_w(\varepsilon) \exp\left(\frac{-\varepsilon}{k_B T}\right) d\left(\frac{\varepsilon}{k_B T}\right),$$

where m is the electron mass, k_B the Boltzmann constant, N_e the electron density, T the electron temperature, ε the incident electron

Table 2. Present fine structure energy levels E in cm^{-1} for the Ar IX ion compared to those of NIST database (Kramida et al. 2018) and to the calculations using the AUTOSTRUCTURE (AS) code performed in Zhou et al. (2015) with their relative errors in per cent.

i	Level	E	NIST	AS	Δ_{NIST}	Δ_{AS}
1	$2s^22p^6\ ^1S_0$	0.0	0.0	0.0	–	–
2	$2s^22p^53s\ ^3P^o_2$	2025916.	2026575.7	2027030.	0.03	0.06
3	$2s^22p^53s\ ^3P^o_1$	2032637.	2033149.7	2034370.	0.03	0.09
4	$2s^22p^53s\ ^3P^o_0$	2043534.	2044543.1	2047200.	0.05	0.18
5	$2s^22p^53s\ ^1P^o_1$	2051373.	2051784.6	2055290.	0.02	0.19
6	$2s^22p^53p\ ^3S_1$	2151874.	2149341.1	2151420.	0.12	0.02
7	$2s^22p^53p\ ^3D_3$	2168394.	2169967.2	2172490.	0.07	0.19
8	$2s^22p^53p\ ^3D_2$	2169522.	2170921.7	2173340.	0.06	0.18
9	$2s^22p^53p\ ^3D_1$	2175108.	2176736.6	2179570.	0.07	0.21
10	$2s^22p^53p\ ^3P_2$	2180703.	2182215.2	2185180.	0.07	0.21
11	$2s^22p^53p\ ^1P_1$	2187558.	2189204.6	2193690.	0.08	0.28
12	$2s^22p^53p\ ^3P_0$	2190478.	2192277.8	2196330.	0.08	0.27
13	$2s^22p^53p\ ^1D_2$	2193499.	2195049.5	2200150.	0.07	0.30
14	$2s^22p^53p\ ^3P_1$	2194337.	2196102.7	2200870.	0.08	0.30
15	$2s^22p^53p\ ^1S_0$	2288771.	2265099.4	2293420.	1.03	0.20
16	$2s^22p^53d\ ^3P^o_0$	2352122.	2349422.	2352970.	0.11	0.04
17	$2s^22p^53d\ ^3P^o_1$	2354168.	2351405.1	2355300.	0.12	0.05
18	$2s^22p^53d\ ^3P^o_2$	2358279.	2355542.7	2360000.	0.12	0.07
19	$2s^22p^53d\ ^3F^o_4$	2360358.	2358778.	2363440.	0.07	0.13
20	$2s^22p^53d\ ^3F^o_3$	2363112.	2361731.2	2366400.	0.06	0.14
21	$2s^22p^53d\ ^3F^o_2$	2368068.	2366940.	2371740.	0.05	0.15
22	$2s^22p^53d\ ^3D^o_3$	2372162.	2384764.	2376010.	0.53	0.16
23	$2s^22p^53d\ ^3D^o_1$	2381926.	2380958.	2386620.	0.04	0.20
24	$2s^22p^53d\ ^3D^o_2$	2383276.	2385174.0	2391820.	0.08	0.36
25	$2s^22p^53d\ ^1F^o_3$	2385911.	2370659.	2391920.	0.64	0.25
26	$2s^22p^53d\ ^1D^o_2$	2386281.	2382377.6	2388840.	0.16	0.11
27	$2s^22p^53d\ ^1P^o_1$	2417832	2411101.4	2424620.	0.28	0.28
28	$2s^22p^54s\ ^3P^o_2$	2700971.	2701052.	–	0	–
29	$2s^22p^54s\ ^1P^o_1$	2703894.	2704217.	–	0.01	–
30	$2s^22p^54s\ ^3P^o_0$	2718599.	–	–	–	–
31	$2s^22p^54s\ ^3P^o_1$	2720540.	2721001.	–	0.02	–

Table 3. Present radiative decay rates A_{ij}, line strengths S, and oscillator strengths f (in absorption form) for the Ar VIII allowed transitions compared to NIST database (Kramida et al. 2018) values and to the MCHF results of Froese Fischer et al. (2006), with their relative errors in per cent. i and j are labelling the levels as in Table 1.

Levels	$A_{ij}(s^{-1})$			S			f		
$i-j$	Present	MCHF	Δ_A	Present	MCHF	Δ_S	Present	MCHF	Δ_f
2 − 1	2.513E + 09	2.427E + 09	3.42	0.910530	0.866400	4.85	1.931E−01	1.847E−01	4.35
3 − 1	2.663E + 09	2.583E + 09	3.00	1.823876	1.738000	4.71	3.942E−01	3.779E−01	4.13
4 − 2	6.592E + 09	6.362E + 09	3.49	1.819126	1.726000	5.12	5.324E−01	5.079E−01	4.60
4 − 3	1.268E + 09	1.222E + 09	3.63	0.364810	0.346200	5.10	5.265E−02	5.022E−02	4.62
5 − 3	7.638E + 09	7.346E + 09	3.82	3.284019	3.114000	5.18	4.745E−01	4.520E−01	4.74
6 − 2	1.130E + 10	1.127E + 10	0.27	0.136381	0.133300	2.26	8.991E−02	8.848E−02	1.59
6 − 3	2.295E + 10	2.251E + 10	1.92	0.282117	0.271300	3.83	9.242E−02	8.947E−02	3.19
7 − 1	1.203E + 10	1.144E + 10	4.90	0.048510	0.045210	6.80	4.609E−02	4.324E−02	6.18
7 − 4	7.533E + 09	7.729E + 09	2.60	0.294917	0.295300	0.13	6.567E−02	6.629E−02	0.94
7 − 6	4.904E + 08	5.170E + 08	5.42	3.468845	3.550000	2.34	2.733E−01	2.824E−01	3.33
8 − 1	1.174E + 10	1.110E + 10	5.45	0.094205	0.087260	7.37	8.965E−02	8.361E−02	6.74
8 − 4	7.485E + 08	7.670E + 08	2.47	0.057999	0.057980	0.03	1.296E−02	1.306E−02	0.77
8 − 5	6.747E + 09	6.911E + 09	2.43	0.523983	0.523300	0.13	7.800E−02	7.856E−02	0.72
8 − 6	5.193E + 08	5.485E + 08	5.62	6.928335	7.096000	2.41	5.566E−01	5.759E−01	3.47
9 − 2	1.348E + 10	1.401E + 10	3.93	0.155546	0.158300	1.77	1.311E−01	1.344E−01	2.51
9 − 3	2.784E + 09	2.816E + 09	1.15	0.032598	0.032300	0.91	1.368E−02	1.364E−02	0.29
9 − 7	1.284E + 09	1.308E + 09	1.87	7.656198	7.642000	0.19	8.045E−01	8.085E−01	0.50
9 − 8	2.453E + 08	2.501E + 08	1.96	1.529750	1.529000	0.05	7.918E−02	7.964E−02	0.58
10 − 3	1.667E + 10	1.691E + 10	1.44	0.292657	0.290700	0.67	1.228E−01	1.228E−01	0
10 − 8	1.478E + 09	1.507E + 09	1.96	13.76576	13.76000	0.04	7.714E−01	7.177E−01	6.96

energy, and

$$\Gamma_w(\varepsilon) = \sum_{J_i^T J_f^T l K_i K_f} \frac{\left[K_i, K_f, J_i^T, J_f^T\right]}{2} \times \begin{Bmatrix} J_i & K_i & l \\ K_f & J_f & 1 \end{Bmatrix}^2 \begin{Bmatrix} K_i & J_i^T & s \\ J_f^T & K_f & 1 \end{Bmatrix}^2 \times \left[1 - \left(\mathrm{Re}\,(S_i)\mathrm{Re}\,(S_f) + \mathrm{Im}\,(S_i)\mathrm{Im}\,(S_f)\right)\right], \quad (1)$$

where $\boldsymbol{L}_i + \boldsymbol{S}_i = \boldsymbol{J}_i, \boldsymbol{J}_i + \boldsymbol{l} = \boldsymbol{K}_i$ and $\boldsymbol{K}_i + \boldsymbol{s} = \boldsymbol{J}_i^T$. The subscript i denotes the initial level (same relations for the final level f). $\boldsymbol{L}$ and $\boldsymbol{S}$ represent the atomic orbital angular momentum and spin of the target, respectively, $\boldsymbol{l}$ is the electron orbital momentum, the superscript T denotes the quantum numbers of the total electron + ion system. S_i (S_f) are the scattering matrix elements for the initial (final) levels, expressed in the intermediate coupling approximation, Re (S) and Im (S) are, respectively, the real and the imaginary parts of the S-matrix element, $\begin{Bmatrix} abc \\ def \end{Bmatrix}$ represent 6–j symbols and we adopt the notation $[x, y, ...] = (2x + 1)(2y + 1)...$ Both S_i and S_f are calculated for the same incident electron energy $\varepsilon = mv^2/2$.

The broadening calculations need the use of atomic and collisional data. First, the atomic structure in intermediate coupling, performed using the SUPERSTRUCTURE (SST) code (Eissner, Jones & Nussbaumer 1974), provides us the atomic data (energy levels, oscillator strengths, radiative decay rates,...), and the Term Coupling Coefficients (TCC) which will be used in a later step. Secondly, the scattering problem in *LS* coupling is carried out using the DISTORTED WAVE (DW) code (Eissner 1998) to provide the reactance matrices **R** in *LS* coupling. It is known that the distorted wave method is adequate for highly charged ions colliding with electrons, because the close collisions are of little importance. The transformed version of the JAJOM code (Saraph 1978) treats the scattering problem in intermediate coupling using the TCC from SST and the matrices **R** from DW to produce collision strengths and **R** in intermediate coupling. The transformed version of JAJOM (Elabidi & Dubau, unpublished results) and the program RTOS (Dubau, unpublished results) transform the reactance matrices to the scattering ones **S**. They also calculate the real (Re **S**) and imaginary (Im **S**) parts of the scattering matrix. The evaluation of Re **S** and Im **S** is carried out according to:

$$\mathrm{Re}\,\mathbf{S} = \left(1 - \mathbf{R}^2\right)\left(1 + \mathbf{R}^2\right)^{-1}, \mathrm{Im}\,\mathbf{S} = 2\mathbf{R}\left(1 + \mathbf{R}^2\right)^{-1} \quad (2)$$

The relation $\mathbf{S} = (1 + i\mathbf{R})(1 - i\mathbf{R})^{-1}$ guarantee the unitarity of the **S**-matrix. The integral in equation (1) is evaluated numerically using the trapezoid method with a variable step of electron energy ε.

3 RESULTS AND DISCUSSIONS

3.1 Atomic structure

Ar VIII is a sodium-like ion, and it has been the interest of several researchers for many years. Many works have been performed for the Ar VIII ion: the energy levels, electric dipole transition rates, oscillator strengths, and radiative lifetimes have been calculated by Natarajan & Mulye (2001) using the Multiconfiguration Dirac–Fock (MCDF) and relativistic Configuration Interaction (CI) with the inclusion of the Breit interaction, quantum electrodynamics, and finite nuclear mass corrections. Froese Fischer, Tachiev & Irimia (2006) have performed calculations of radiative atomic data for the sodium-like to argon-like sequences using the Multiconfiguration Hartree–Fock (MCHF) method. Liang, Whiteford & Badnell (2009) have studied the inner-shell electron-impact excitation of all Na-like ions from Mg^+ to Kr^{25+} (included Ar^{7+}) by using the intermediate-coupling frame transformation R-matrix method with both Auger and radiation damping included via the optical potential approach. Breit–Pauli R-matrix electron-impact excitation calculations have

Table 4. Present radiative decay rates A_{ij}, line strengths S, and weighted oscillator strengths gf for some Ar IX allowed transitions compared to the calculations with AUTOSTRUCTURE code performed in Zhou et al. (2015) (AS) and to the CI relativistic calculations in Jönsson et al. (2014) (CI). i and j are labelling the levels as in Table 2.

Levels	$A_{ij}(s^{-1})$			S		gf		
$i-j$	Present	AS	CI	Present	AS	Present	AS	CI
3 − 1	5.981E + 10	5.100E + 10	6.255E + 10	0.010545	0.008969	6.511E−02	1.210E−01	6.807E−02
5 − 1	1.607E + 11	1.301E + 11	1.581E + 11	0.027572	0.022190	1.718E−01	1.385E−01	1.689E−01
6 − 2	1.259E + 09	1.097E + 09	9.763E + 08	0.933187	0.844044	3.570E−01	3.189E−01	2.899E−01
6 − 3	2.642E + 08	2.142E + 08	2.097E + 08	0.230728	0.197793	8.357E−02	7.032E−02	6.950E−02
6 − 4	5.585E + 07	4.125E + 07	4.298E + 07	0.065030	0.053954	2.140E−02	1.708E−02	1.748E−02
6 − 5	2.504E + 07	2.052E + 07	2.127E + 07	0.036528	0.034215	1.115E−02	9.990E−03	9.988E−03
7 − 2	2.367E + 09	2.513E + 09	2.260E + 09	2.827374	2.820873	1.224E+00	1.246E+00	1.149E+00
8 − 2	1.040E + 09	1.104E + 09	9.593E + 08	0.866751	0.870326	3.781E−01	3.868E−01	3.439E−01
8 − 3	1.193E + 09	1.246E + 09	1.117E + 09	1.147760	1.145448	4.772E−01	4.835E−01	4.603E−01
8 − 5	3.631E + 06	5.161E + 06	4.576E + 06	0.005433	0.007743	1.950E−03	2.777E−03	2.406E−03
9 − 2	3.112E + 08	3.693E + 08	3.252E + 08	0.138776	0.154051	6.289E−02	7.138E−02	6.465E−02
9 − 3	1.814E + 09	1.976E + 09	1.763E + 09	0.928862	0.955940	4.020E−01	4.216E−01	3.834E−01
9 − 4	1.866E + 08	1.454E + 08	1.687E + 08	0.121273	0.092789	4.847E−02	3.731E−02	4.323E−02
9 − 5	3.486E + 06	4.929E + 06	4.509E + 06	0.002725	0.003802	1.024E−03	1.435E−03	1.294E−03
10 − 2	1.526E + 09	1.739E + 09	1.555E + 09	1.015761	1.084970	4.776E−01	5.212E−01	4.797E−01
10 − 3	9.759E + 08	1.052E + 09	9.050E + 08	0.741953	0.757252	3.337E−01	3.469E−01	3.044E−01
10 − 5	2.020E + 08	1.848E + 08	2.106E + 08	0.230411	0.208177	9.052E−02	8.213E−02	9.247E−02
11 − 2	4.894E + 07	4.174E + 07	3.913E + 07	0.017159	0.013353	8.425E−03	6.760E−03	6.640E−03
11 − 3	6.301E + 07	5.582E + 07	6.820E + 07	0.025094	0.020440	1.181E−02	9.891E−03	1.257E−03
11 − 4	1.167E + 09	1.266E + 09	1.064E + 09	0.578615	0.596240	2.531E−01	2.653E−01	2.279E−01
11 − 5	9.567E + 08	1.024E + 09	1.004E + 09	0.560871	0.572107	2.320E−01	2.405E−01	2.385E−01
12 − 3	2.473E + 09	2.775E + 09	2.517E + 09	0.310337	0.322431	1.488E−01	1.586E−01	1.486E−01
12 − 5	4.413E + 08	5.046E + 08	4.238E + 08	0.080920	0.088785	3.419E−02	3.804E−02	3.209E−02
13 − 2	1.704E + 08	1.871E + 08	2.045E + 08	0.089347	0.089001	4.548E−02	4.680E−02	5.386E−02
13 − 3	2.109E + 08	2.345E + 08	2.211E + 08	0.125014	0.127483	6.109E−02	6.420E−02	6.309E−02
13 − 5	2.091E + 09	2.244E + 09	2.006E + 09	1.797761	1.821448	7.761E−01	8.015E−01	7.304E−01
14 − 2	4.488E + 08	5.745E + 08	5.442E + 08	0.139107	0.161938	7.117E−02	8.551E−02	8.498E−02
14 − 3	5.587E + 07	3.891E + 07	4.173E + 07	0.019567	0.012482	9.611E−03	6.313E−03	7.054E−03
14 − 4	1.020E + 09	1.135E + 09	1.051E + 09	0.440523	0.463250	2.018E−01	2.162E−01	2.051E−01
14 − 5	1.133E + 09	1.202E + 09	1.047E + 09	0.574088	0.576861	2.493E−01	2.551E−01	2.256E−01
15 − 3	3.185E + 09	3.698E + 09	2.328E + 09	0.093540	0.105006	7.278E−02	8.263E−02	6.448E−02
15 − 5	9.390E + 09	9.918E + 09	6.904E + 09	0.346394	0.362516	2.498E−01	2.622E−01	2.259E−01
16 − 6	5.485E + 09	5.276E + 09	4.604E + 09	0.337162	0.318049	2.051E−01	1.947E−01	1.726E−01
16 − 9	5.724E + 08	4.574E + 08	4.399E + 08	0.050936	0.043306	2.739E−02	2.281E−02	2.212E−02
16 − 11	9.158E + 07	8.019E + 07	–	0.010143	0.009794	5.070E−03	4.738E−03	–
16 − 14	5.095E + 08	4.366E + 08	4.702E + 08	0.064019	0.061236	3.068E−02	2.829E−02	2.998E−02
17 − 1	5.517E + 09	5.711E + 09	6.047E + 09	0.000626	0.000647	4.477E−03	4.630E−03	4.919E−03
17 − 6	4.875E + 09	4.745E + 09	4.143E + 09	0.871983	0.829027	5.358E−01	5.134E−01	4.573E−01
17 − 8	3.832E + 08	2.852E + 08	2.550E + 08	0.090142	0.070086	5.056E−02	3.874E−02	3.526E−02
17 − 9	7.219E + 07	9.142E + 07	6.856E + 07	0.018619	0.024947	1.013E−02	1.332E−02	1.012E−02
17 − 10	6.660E + 08	5.843E + 08	5.360E + 08	0.188933	0.175713	9.955E−02	9.080E−02	8.434E−02
17 − 11	6.823E + 07	3.949E + 07	–	0.021844	0.013851	1.106E−02	6.799E−03	–
17 − 12	3.021E + 08	2.502E + 08	–	0.101976	0.092223	5.070E−02	4.453E−02	–
17 − 13	9.744E + 07	9.322E + 07	–	0.034785	0.036962	1.698E−02	1.742E−02	–
17 − 14	1.603E + 08	1.395E + 08	–	0.058143	0.056100	2.823E−02	2.632E−02	2.864E−02
18 − 6	3.632E + 09	3.604E + 09	3.187E + 09	1.019249	0.980050	6.390E−01	6.209E−01	5.629E−01
18 − 7	1.966E + 08	1.290E + 08	1.244E + 08	0.070864	0.048283	4.087E−02	2.750E−02	2.711E−02
18 − 8	2.142E + 08	2.206E + 08	1.483E + 08	0.078587	0.083697	4.506E−02	4.746E−02	3.266E−02
18 − 9	2.248E + 08	2.207E + 08	1.984E + 08	0.090276	0.092734	5.023E−02	5.082E−02	4.659E−02
18 − 10	1.826E + 09	1.664E + 09	1.468E + 09	0.804805	0.768705	4.341E−01	4.082E−01	3.669E−01
18 − 11	9.863E + 07	7.021E + 07	–	0.048915	0.037665	2.537E−02	1.903E−02	–
18 − 13	2.750E + 08	2.110E + 08	–	0.151680	0.127490	7.592E−02	6.190E−02	–
18 − 14	8.301E + 07	5.954E + 07	6.469E + 07	0.046494	0.036463	2.315E−02	1.762E−02	1.909E−02
19 − 7	6.619E + 09	6.299E + 09	5.652E + 09	4.156665	4.018435	2.424E+00	2.331E+00	2.143E+00
20 − 7	1.004E + 09	9.854E + 08	8.250E + 08	0.470007	0.466846	2.780E−01	2.750E−01	2.358E−01
20 − 8	5.747E + 09	5.506E + 09	4.990E + 09	2.736707	2.643177	1.609E+00	1.550E+00	1.441E+00
20 − 10	4.530E + 07	2.972E + 07	4.054E + 07	0.025789	0.017252	1.429E−02	9.497E−03	1.322E−02

Table 5. Our Stark widths (Q) in Å for 14 Ar VIII lines at electron density $N = 10^{19}$ cm^{-3} compared to the semiclassical perturbation results (SCP) obtained in Dimitrijević & Sahal-Bréchot (1999). Δ is the relative errors in per cent. Temperature values are given in 10^5 K.

Transition	T	Q	SCP	Δ	Transition	T	Q	SCP	Δ
	2	9.309E−02	9.30E−02	00		2	2.222E−02	1.19E−02	46
3p $^2P^\circ_{1/2}$ − 3s $^2S_{1/2}$	5	6.804E−02	6.14E−02	10	4p $^2P^\circ_{1/2}$ − 3s $^2S_{1/2}$	5	1.341E−02	8.15E−03	39
λ_{SST} = 715.68 Å	10	5.313E−02	4.64E−02	13	λ_{SST} = 159.66 Å	10	8.750E−03	6.38E−03	27
2-1	15	4.534E−02	4.00E−02	12	7-1	15	6.700E−03	5.62E−03	16
	20	4.014E−02	3.62E−02	10		20	5.510E−03	5.16E−03	06
	30	3.325E−02	3.17E−03	05		30	4.140E−03	4.62E−03	12
	2	8.951E−02	8.99E−02	01		2	1.783E−02	1.19E−02	33
3p $^2P^\circ_{3/2}$ − 3s $^2S_{1/2}$	5	6.540E−02	5.93E−02	09	4p $^2P^\circ_{3/2}$ − 3s $^2S_{1/2}$	5	1.106E−02	8.15E−03	26
λ_{SST} = 702.39 Å	10	5.107E−02	4.48E−02	12	λ_{SST} = 159.41 Å	10	7.510E−03	6.38E−03	15
3-1	15	4.359E−02	3.86E−02	11	8-1	15	5.900E−03	5.62E−03	05
	20	3.859E−02	3.50E−02	09		20	4.940E−03	5.16E−03	05
	30	3.196E−02	3.07E−02	04		30	3.790E−03	4.62E−03	22
	2	3.234E−01	5.73E−02	82		2	2.922E+00	2.10E+00	28
3d $^2D_{1/2}$ − 3p $^2P^\circ_{1/2}$	5	1.734E−01	3.79E−02	78	4p $^2P^\circ_{3/2}$ − 4s $^2S_{1/2}$	5	2.087E+00	1.47E+00	30
λ_{SST} = 517.63 Å	10	9.257E−02	2.87E−02	69	λ_{SST} = 1886.0 Å	10	1.496E+00	1.17E+00	22
4-2	15	6.176E−02	2.48E−02	60	8-6	15	1.189E+00	1.03E+00	13
	20	4.609E−02	2.25E−02	51		20	9.961E−01	9.52E−01	04
	30	3.057E−02	1.98E−02	35		30	7.598E−01	8.52E−01	12
	2	2.620E−01	5.91E−02	77		2	3.659E+00	–	–
3d $^2D_{1/2}$ − 3p $^2P^\circ_{3/2}$	5	1.427E−01	3.91E−02	73	4p $^2P^\circ_{1/2}$ − 4s $^2S_{1/2}$	5	2.805E+00	–	–
λ_{SST} = 524.82 Å	10	7.828E−02	2.96E−02	62	λ_{SST} = 1922.4 Å	10	1.960E+00	–	–
4-3	15	5.334E−02	2.55E−02	52	7-6	15	1.512E+00	–	–
	20	4.045E−02	2.32E−02	43		20	1.238E+00	–	–
	30	2.746E−02	2.04E−02	26		30	9.150E−01	–	–
	2	2.507E−01	–	–		2	1.757E−01	–	–
3d $^2D_{5/2}$ − 3p $^2P^\circ_{3/2}$	5	1.329E−01	–	–	4p $^2P^\circ_{1/2}$ − 3d $^2D_{3/2}$	5	9.666E−02	–	–
λ_{SST} = 524.21 Å	10	7.180E−02	–	–	λ_{SST} = 340.82 Å	10	5.611E−02	–	–
5-3	15	4.880E−02	–	–	7-4	15	3.991E−02	–	–
	20	3.705E−02	–	–		20	3.117E−02	–	–
	30	2.529E−02	–	–		30	2.191E−02	–	–
	2	3.364E−02	1.61E−02	52		2	1.604E−01	–	–
4s $^2S_{1/2}$ −3p $^2P^\circ_{1/2}$	5	2.126E−02	1.12E−02	47	4p $^2P^\circ_{3/2}$ − 3d $^2D_{3/2}$	5	8.769E−02	–	–
λ_{SST} = 230.11 Å	10	1.473E−02	8.80E−03	40	λ_{SST} = 339.66 Å	10	5.100E−02	–	–
6-2	15	1.173E−02	7.73E−03	34	8-4	15	3.649E−02	–	–
	20	9.900E−03	7.08E−03	28		20	2.866E−02	–	–
	30	7.690E−03	6.28E−03	18		30	2.033E−02	–	–
	2	3.402E−02	1.64E−02	52		2	1.466E−01	5.47E−02	63
4s $^2S_{1/2}$ −3p $^2P^\circ_{3/2}$	5	2.149E−02	1.14E−02	47	4p $^2P^\circ_{3/2}$ − 3d $^2D_{5/2}$	5	7.959E−02	3.76E−02	53
λ_{SST} = 231.52 Å	10	1.489E−02	8.93E−03	40	λ_{SST} = 339.91 Å	10	4.657E−02	2.95E−02	37
6-3	15	1.186E−02	7.84E−03	34	8-5	15	3.359E−02	2.60E−02	21
	20	1.001E−02	7.18E−03	28		20	2.658E−02	2.39E−02	10
	30	7.770E−03	6.37E−03	18		30	1.904E−02	2.14E−02	12

been carried out for a number of ion stages along the argon isonuclear sequence by Ludlow et al. (2010).

The Ar IX ion belongs to the neon isoelectronic sequence. Because of their closed-shell nature, Ne-like ions have wide applications in laboratory experiments, astrophysics, and plasma physics. Ar IX is the dominant argon ion species in laboratory and cosmic plasmas (Zhou et al. 2015). The study of the Ar IX spectrum started many years ago. Crance (1973) has calculated radiative decay rates for some transitions for neon-like ions from Si V to Ni XIX using a central-field approach. Fawcett, Ridgeley & Bromage (1978) have analysed some spectroscopic observations where 80 new Ar IX energy levels are established. Fawcett (1984) computed weighted oscillator strengths and energy levels for ions in the neon isoelectronic sequence between Al IV and Ar IX by the Hartree–Fock–Relativistic and Blume-Watson methods taking into account configuration interaction. Jönsson et al. (2014) have published energies, transition rates, oscillator strengths, and lifetimes from relativistic configuration interaction calculations of the $2p^6$, $2p^5 3s$, $2p^5 3p$, and $2p^5 3d$ configurations in all Ne-like ions from Mg^{2+} to Kr^{26+}. Scattering calculations for Ar IX have been done in Mohan, Le Dourneuf & Hibbert (1991) using the configuration interaction code CIV3 of Hibbert (1975). The newest structure calculations for Ar IX are those of Zhou et al. (2015), where the authors have calculated, besides the energy levels and the atomic radiative data, Breit–Pauli distorted wave collision strengths for four electron energies 75, 125, 175, and 250 Ryd.

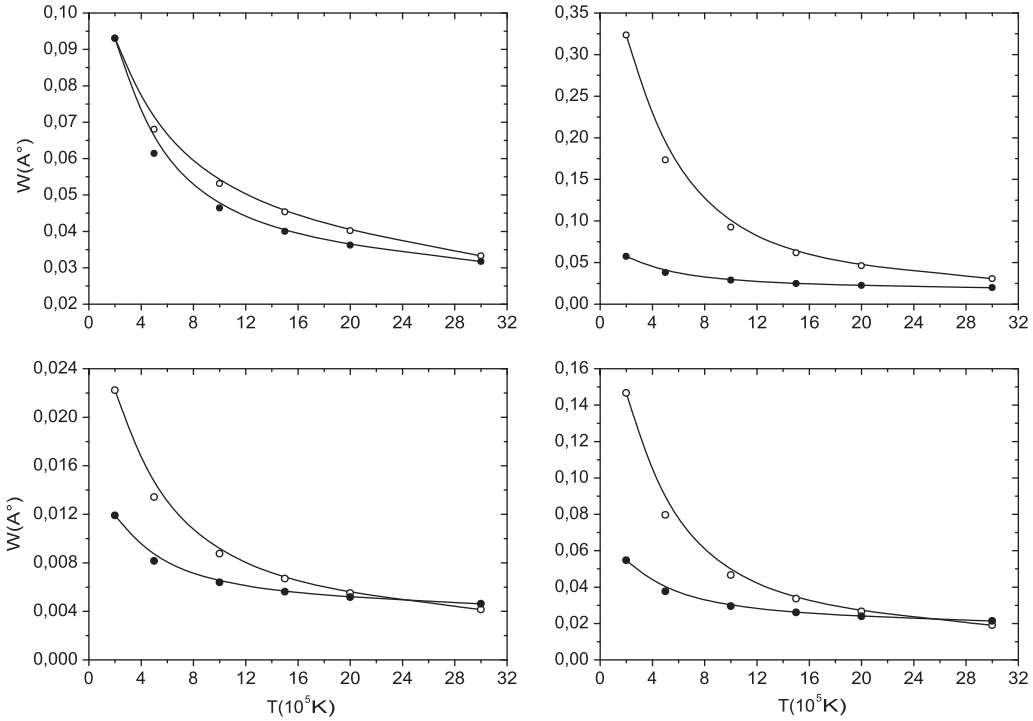

Figure 1. Our Stark width (open circles) and those of the SCP (Dimitrijević & Sahal-Bréchot 1999) method (solid circles) as a function of electron temperature for four Ar VIII transitions: $3p\ ^2P^o_{1/2} - 3s\ ^2S_{1/2}$ (left-up), $3d\ ^2D_{1/2} - 3p\ ^2P^o_{1/2}$ (right-up), $4p\ ^2P^o_{1/2} - 3s\ ^2S_{1/2}$ (left-down), and $4p\ ^2P^o_{3/2} - 3d\ ^2D_{5/2}$ (right-down). Electron density is $N_e = 10^{19}$ cm^{-3}.

We have used in our calculations six configurations for Ar VIII: $1s^22s^22p^6$(3s, 3p, 3d, 4s, 4p, 4d) giving rise to 10 fine structure levels. For the Ar IX, we have used the following five configurations: $1s^2(2s^22p^6, 2s^22p^53s, 2s^22p^53p, 2s^22p^53d, 2s^22p^54s)$ giving rise to 31 fine structure levels. The energy levels of Ar VIII are reported in Table 1 and compared to those from the NIST database (Kramida et al. 2018) and to those of the MCHF method (Froese Fischer et al. 2006). The average agreement is about 0.3 per cent with the NIST values and about 0.5 per cent with the MCHF ones. The energies of Ar IX are reported in Table 2. They are compared to NIST values (Kramida et al. 2018) where the average agreement is about 0.1 per cent and to the calculations using the AUTOSTRUCTURE code (Badnell 2011) performed in Zhou et al. (2015), where the average agreement is about 0.2 per cent. The radiative data (including radiative decay rates, line strengths, and oscillator strengths) are presented in Table 3 for Ar VIII and in Table 4 for Ar IX. The same comparisons as for the energies have been performed for the radiative data. We found an agreement of about 3 per cent for Ar VIII and 5 per cent for Ar IX for all the calculated parameters. The above comparisons show that we can trust our preliminary data which will be used for the broadening calculations.

3.2 Line broadening results

The essence of the present work is to provide Stark broadening data for the ions Ar VIII and Ar IX necessary for astrophysics and laboratory plasma diagnostics and modelling. Even the atomic structure of these two ions are numerous, Stark broadening ones are missing or few. For Ar VIII, there are only the semiclassical results (SCP) of Dimitrijević & Sahal-Bréchot (1999). To the best of our knowledge, there are no Stark broadening results in the literature for Ar IX.

The Stark widths of 14 Ar VIII spectral lines are presented in Table 5. We compare our results to the semiclassical ones of Dimitrijević & Sahal-Bréchot (1999) for electron temperature ranging from 2×10^5 K to 3×10^6 K at an electron density $N = 10^{19}$ cm^{-3}. The two resonance lines $3p\ ^2P{-}3s\ ^2S$ present good agreement with the SCP results, it is about 8 per cent. For the other lines (except the 3d−3p and 4p−3d ones) the errors are in general decreasing with electron temperature, and varying between 18 and 37 per cent, with an average of about 27 per cent. The transitions 3d−3p and 4p−3d (4 − 2, 4 − 3 and 8 − 5 in Table 5) involve the level 3d. The disagreement between the quantum and SCP calculations can reach 80 per cent. This might be because we did not take into account the perturbers of the level 3d due to some numerical obstacles in the scattering calculations. The general difference between quantum and SCP results may come from the difference in the used atomic data. Our atomic data are calculated using the UCL codes SST/DW/JAJOM during the broadening calculations, while those used in the SCP calculations of Dimitrijević & Sahal-Bréchot (1999) are taken from Bashkin & Stoner (1978). We have shown (Elabidi, Sahal-Bréchot & Dimitrijević 2014; Aloui et al. 2018) that disagreements between quantum and SCP results can come from the estimation of the strong collision contributions to line widths. We present in Fig. 1 our Stark widths and the SCP ones as a function of electron temperature and at electron density $N = 10^{19}$ cm^{-3} for 4 Ar VIII lines: $3p\ ^2P^\circ_{1/2} - 3s\ ^2S_{1/2}$ (2–1), $3d\ ^2D_{1/2} - 3p\ ^2P^\circ_{1/2}$ (4–2), $4p\ ^2P^\circ_{1/2} - 3s\ ^2S_{1/2}$ (7–1), and $4p\ ^2P^\circ_{3/2} - 3d\ ^2D_{5/2}$ (8–5). The Stark broadening for 16 Ar IX spectral lines are presented in Table 6 for the same temperature range as for Ar VIII. No results in the literature to compare with. Experimental or/and other theoretical evaluations of Ar IX

Table 6. Our quantum Stark widths Q for 16 Ar IX lines at electron density $N = 10^{19}$ cm^{-3}.

Transition	$T(10^5$ K)	Q(Å)	Transition	$T(10^5$ K)	Q(Å)
	2	3.563E−04		2	8.062E−02
$2p^6\ ^1S_0 - 2p^5 3s\ ^1P^\circ_1$	5	2.278E−04	$2p^5 3d\ ^3P^\circ_0 - 2p^5 3p\ ^3D_1$	5	5.256E−02
λ_{SST} =48.75 Å	10	1.613E−04	λ_{SST} =564.93 Å	10	3.527E−02
5-1	15	1.310E−04	16-9	15	2.649E−01
	20	1.126E−04		20	2.111E−01
	30	9.041E−05		30	1.480E−01
	2	9.623E−02		2	4.976E−01
$2p^5 3p\ ^3S_1 - 2p^5 3s\ ^3P^\circ_2$	5	8.067E−02	$2p^5 3d\ ^3P^\circ_1 - 2p^5 3p\ ^3S_1$	5	3.310E−01
λ_{SST} =793.91 Å	10	6.901E−02	λ_{SST} =494.33 Å	10	2.218E−01
6-2	15	5.931E−02	17-6	15	1.652E−01
	20	5.189E−02		20	1.306E−01
	30	4.174E−02		30	9.059E−02
	2	1.076E−01		2	5.110E−01
$2p^5 3p\ ^3S_1 - 2p^5 3s\ ^3P^\circ_1$	5	9.020E−02	$2p^5 3d\ ^3P^\circ_1 - 2p^5 3p\ ^3D_2$	5	3.414E−01
λ_{SST} =838.66 Å	10	7.733E−02	λ_{SST} =541.58 Å	10	2.320E−01
6-3	15	6.654E−02	17-8	15	1.751E−01
	20	5.824E−02		20	1.400E−01
	30	4.686E−02		30	9.869E−02
	2	1.304E−01		2	6.213E−01
$2p^5 3p\ ^3S_1 - 2p^5 3s\ ^3P^\circ_0$	5	1.096E−01	$2p^5 3d\ ^3P^\circ_1 - 2p^5 3p\ ^3D_1$	5	4.099E−01
λ_{SST} =923.02 Å	10	9.437E−02	λ_{SST} =558.47 Å	10	2.765E−01
6-4	15	8.132E−02	17-9	15	2.080E−01
	20	7.120E−02		20	1.656E−01
	30	5.727E−02		30	1.117E−01
	2	8.368E−02		2	3.239E−01
$2p^5 3p\ ^3D_3 - 2p^5 3s\ ^3P^\circ_2$	5	6.383E−02	$2p^5 3d\ ^3P^\circ_2 - 2p^5 3p\ ^3S_1$	5	2.223E−01
λ_{SST} =701.86 Å	10	5.110E−02	λ_{SST} =484.48 Å	10	1.487E−01
7-2	15	4.356E−02	18-6	15	1.084E−01
	20	3.828E−02		20	8.348E−02
	30	3.119E−02		30	5.504E−02
	2	8.975E−02		2	3.312E−01
$2p^5 3p\ ^3D_2 - 2p^5 3s\ ^3P^\circ_2$	5	7.692E−02	$2p^5 3d\ ^3P^\circ_2 - 2p^5 3p\ ^3D_3$	5	2.303E−01
λ_{SST} =696.35 Å	10	6.482E−02	λ_{SST} =526.63 Å	10	1.556E−01
8-2	15	5.570E−02	18-7	15	1.154E−01
	20	4.883E−02		20	9.079E−02
	30	3.925E−02		30	6.270E−02
	2	9.978E−02		2	3.437E−01
$2p^5 3p\ ^3D_2 - 2p^5 3s\ ^3P^\circ_1$	5	8.659E−02	$2p^5 3d\ ^3P^\circ_2 - 2p^5 3p\ ^3D_2$	5	2.396E−01
λ_{SST} =730.54 Å	10	7.339E−02	λ_{SST} =529.78 Å	10	1.631E−01
8-3	15	6.314E−02	18-8	15	1.217E−01
	20	5.535E−02		20	9.629E−02
	30	4.444E−02		30	6.696E−02
	2	6.351E−01		2	4.080E−01
$2p^5 3d\ ^3P^\circ_0 - 2p^5 3p\ ^3S_1$	5	4.149E−01	$2p^5 3d\ ^3P^\circ_2 - 2p^5 3p\ ^3D_1$	5	2.850E−01
λ_{SST} =499.38 Å	10	2.762E−01	λ_{SST} =545.94 Å	10	1.949E−01
16-6	15	2.055E−01	18-9	15	1.459E−01
	20	1.624E−01		20	1.157E−01
	30	1.126E−01		30	8.064E−02

line broadening will be very welcome to test our results, and consequently, can be used with trust in plasmas modelling and diagnostics.

4 STARK BROADENING EFFECT IN WHITE DWARF ATMOSPHERES

Since ionized argon spectral lines are observed in hot DO white dwarfs spectra (Werner, Rauch & Kruk 2017), and in order to prove the importance of our calculated electron impact Stark widths, we have investigated the influence of Stark broadening in such stars. Stark widths are compared with thermal Doppler widths as a function of atmospheric layer temperatures for different stellar atmospheres. Doppler widths are calculated using eq. (21) of Konjević (1999). We use the model atmospheres of Wesemael (1981) which are LTE models assuming plane-parallel geometry and pure helium composition.

In Figs 2–4, we illustrate the importance of electron impact broadening in DO white dwarfs atmospheres. In Fig. 2, we present Stark and Doppler widths for Ar VIII $4p\ ^2P^\circ_{3/2} - 4s\ ^2S_{1/2}$ ($\lambda = 1886.0$

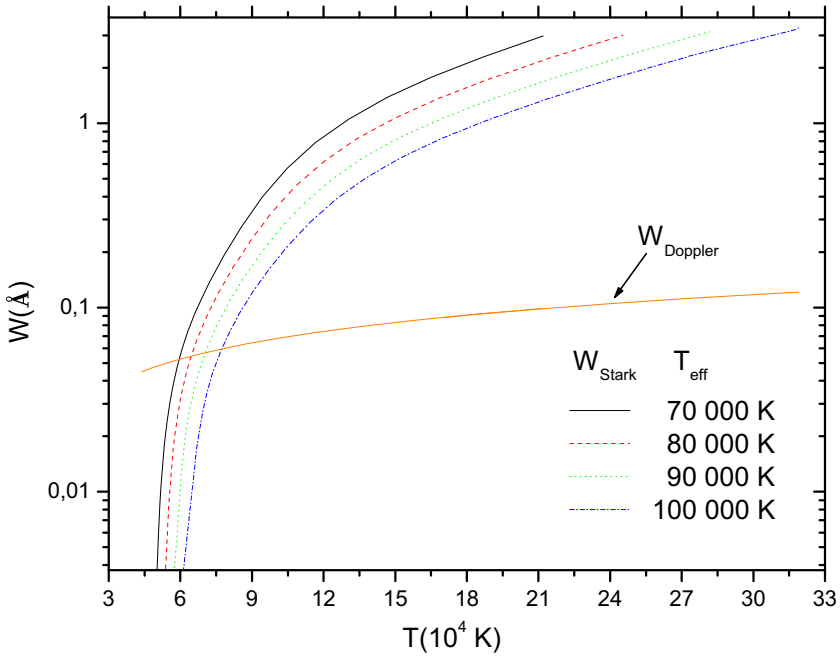

Figure 2. Stark and Doppler widths for Ar VIII $4p\ ^2P^\circ_{3/2} - 4s\ ^2S_{1/2}$ ($\lambda = 1886.0$ Å) spectral line as a function of atmospheric layer temperatures. Stark ($W_{\rm Stark}$) and Doppler ($W_{\rm Doppler}$) widths are shown for four atmospheric models (Wesemael 1981) with effective temperature T_{eff} =70 000 K to 100 000 K and $\log g = 8$.

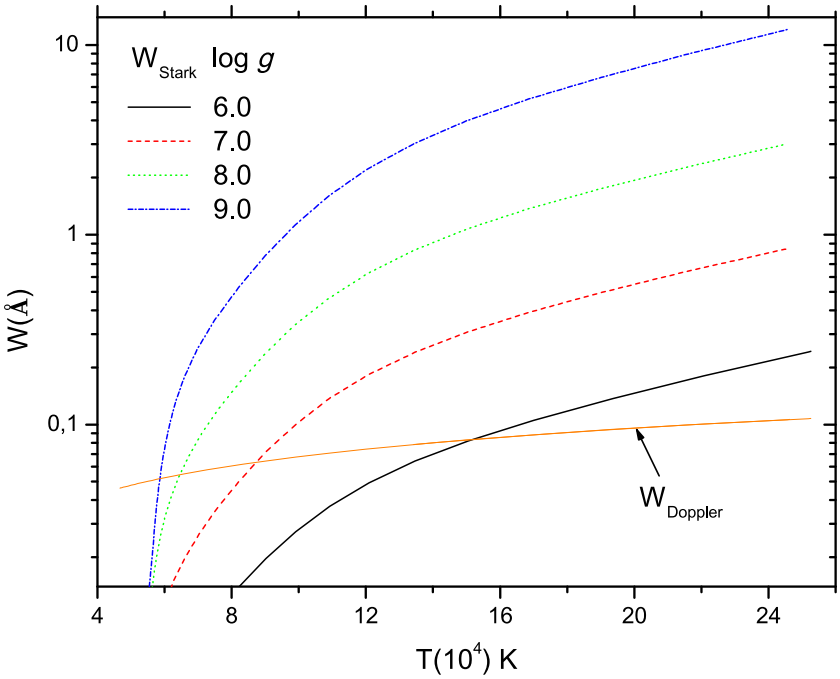

Figure 3. Stark and Doppler widths for Ar VIII $4p\ ^2P^\circ_{3/2} - 4s\ ^2S_{1/2}$ ($\lambda = 1886.0$ Å) spectral line as a function of atmospheric layers temperatures. Stark ($W_{\rm Stark}$) and Doppler ($W_{\rm Doppler}$) widths are shown for four atmospheric models (Wesemael 1981) with $\log g = 6$ to 9 and effective temperature T_{eff} =80 000 K.

Å) spectral line as a function of atmospheric layer temperatures. Stark and Doppler widths are shown for four atmospheric models (Wesemael 1981) with effective temperature $T_{\rm eff} = 70\,000$ K to 100 000 K and $\log g = 8$. It is clearly seen from Fig. 2 that Stark broadening is the dominant broadening mechanism for all studied atmospheres. We can see also that, at the deepest atmospheric layers, Stark width is about two orders of magnitude greater than Doppler width. In Fig. 3, we show Stark and Doppler widths for Ar VIII $4p\ ^2P^\circ_{3/2} - 4s\ ^2S_{1/2}$ ($\lambda = 1886.0$ Å) spectral line as a function of atmospheric layer temperatures. Stark and Doppler widths are shown for four atmospheric models (Wesemael 1981) with $\log g = 6$–9 and effective temperature $T_{\rm eff} = 80\,000$ K. We can see from Fig. 3 that for the atmosphere with $\log g = 6$, Stark broadening becomes dominant comparing with Doppler one from

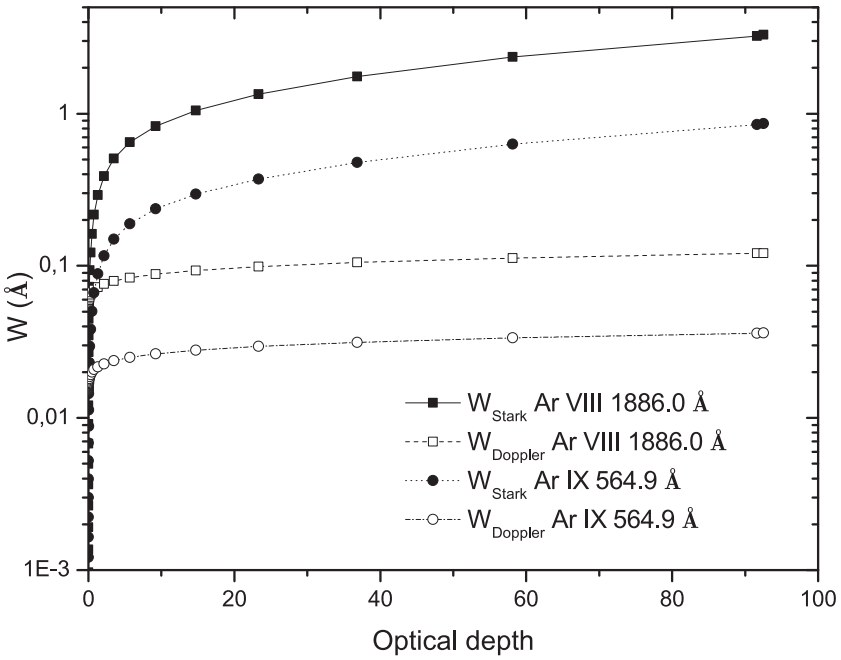

Figure 4. Stark and Doppler widths for Ar VIII $4p\ ^2P^\circ_{3/2} - 4s\ ^2S_{1/2}$ ($\lambda = 1886.0$ Å) and Ar IX $3d\ ^3P^\circ_0 - 3p\ ^3D_1$ ($\lambda = 564.93$ Å) spectral lines as a function of Rosseland optical depth. Stark an Doppler widths are shown for an atmospheric model (Wesemael 1981) with effective temperature T_{eff} =100 000 K and $\log g = 8$.

the atmospheric layer with temperature $T \approx 150\,000$ K. At the deepest atmospheric layer ($T \approx 252\,000$ K), Stark width is twice the Doppler one. For the atmospheres with $\log g = 7$ to $\log g = 9$, Stark broadening is the dominant broadening mechanism nearly for all atmospheric layers. Stark width is two orders of magnitude greater than Doppler one for the deepest atmospheric layer of the atmosphere with $\log g = 9$. In Fig. 4, we present Stark and Doppler widths for Ar VIII $4p\ ^2P^\circ_{3/2} - 4s\ ^2S_{1/2}$ ($\lambda = 1886.0$ Å) and Ar IX $3d\ ^3P^\circ_0 - 3p\ ^3D_1$ ($\lambda = 564.93$ Å) spectral lines as a function of Rosseland optical depth. Stark and Doppler widths are shown for an atmospheric model (Wesemael 1981) with effective temperature $T_{\rm eff}$ =100 000 K and $\log g = 8$. As one can see, for the plasma conditions of the considered DO white dwarf atmosphere, Stark broadening is much more important than thermal Doppler one.

5 CONCLUSIONS

Using our quantum mechanical method, we have calculated in the present work Stark broadening data for 14 Ar VIII and 16 Ar IX lines. Calculations have been made for the temperature range $2 \times 10^5 - 3 \times 10^6$ K and at an electron density $N = 10^{19}$ cm^{-3}, useful for the development of the spectral analysis using the NLTE model atmosphere techniques. Our Ar VIII results have been compared to the semiclassical calculations of Dimitrijević & Sahal-Bréchot (1999), and an average agreement of about 27 per cent has been found. Higher disagreement has been found for three transitions involving the 3d levels (3d−3p and 4p−3d). The general difference between Q and SCP calculations may arise from two sources: first, the difference in the used atomic data and secondly from the evaluation of strong collision contributions to Stark broadening. The Stark broadening of the Ar IX lines are missing in the literature and our results come to fill this lack. Consequently, they may solve some of the problems cited in Rauch et al. (2007) and seem related to the lack of line broadening data. We study also the importance of Stark broadening effects compared to other mechanisms of broadening such as the Doppler (thermal) one. We find that Stark broadening mechanism is dominant compared with Doppler one for nearly all atmospheric layers of the studied atmospheres of hot DO white dwarfs. The influence of Stark broadening increases with log g. Our work suggests that accurate Stark broadening parameters for highly charged argon ions will be for interest for the investigation of hot white dwarfs and the determination of abundance of argon in such stars. We provide also some of our atomic data (energy levels, oscillator strengths, radiative decay rates, and line strengths) used in our line broadening calculations. We compare them to the Multiconfiguration Dirac–Hartree–Fock (Froese Fischer et al. 2006) ones, to the calculations performed in Zhou et al. (2015) using the AUTOSTRUCTURE code, and to the CI relativistic calculations (Jönsson et al. 2014). Good agreement has been found between our results and the three other ones. These comparisons are important in testing our intermediate results. We hope that the present calculations can be useful in stellar spectroscopy, and in particular in astrophysical and laboratory plasmas analysis.

ACKNOWLEDGEMENTS

This work has been supported by the Tunisian Laboratory of Molecular Spectroscopy and Dynamics LR18ES02 and the French Research Unit UMR 8112. It has also been supported by the Paris Observatory and the CNRS. We also acknowledge financial support from the 'Programme National de Physique Stellaire' (PNPS) of CNRS/INSU, CEA and CNES, France.

REFERENCES

Aloui R., Elabidi H., Sahal-Bréchot S., Dimitrijević M. S., 2018, Atoms, 6, 20

Badnell N. R., 2011, Comput. Phys. Commun., 182, 1528

Barstow M. A., Hubeny I., Holberg J. B., 1998, MNRAS, 299, 520
Bashkin S., Stoner J. O., Jr., 1975, in Atomic Energy levels and Grotrian Diagrams, vol2, North Holland, Amsterdam
Crance M., 1973, At. Data Nucl. Data Tables, 5, 185
Dimitrijević M. S., 2003, Astron. Astrophys. Trans., 22, 389
Dimitrijević M. S., Sahal-Bréchot S., 1999, Serb. Astron. J., 160, 15
Eissner W., 1998, Comput. Phys. Comm., 114, 295
Eissner W., Jones M., Nussbaumer H., 1974, Comput. Phys. Commun., 8, 270
Elabidi H., Sahal-Bréchot S., 2011, Eur. Phys. J. D., 61, 258
Elabidi H., Sahal-Bréchot S., 2018, MNRAS, 480, 697
Elabidi H., Ben Nessib N., Sahal-Bréchot S., 2004, J. Phys. B: At. Mol. Phys., 37, 63
Elabidi H., Ben Nessib N., Cornille M., Dubau J., Sahal-Bréchot S., 2008, J. Phys. B: At. Mol. Phys., 41, 025702
Elabidi H., Sahal-Bréchot S., Dimitrijević M. S., Ben Nessib N., 2011, MNRAS, 417, 2624
Elabidi H., Sahal-Bréchot S., Dimitrijević M. S., 2014, Adv. Space Res., 54, 1184
Fawcett B. C., 1984, Phys. Scr., 30, 326
Fawcett B. C., Ridgeley A., Bromage G. E., 1978, Phys. Scr., 18, 315
Froese Fischer C., Tachiev G., Irimia A., 2006, At. Data Nucl. Data Tables, 92, 607
Hibbert A., 1975, Comput. Phys. Comm., 9, 141
Jönsson P. et al., 2014, At. Data Nucl. Data Tables, 100, 1
Konjević N., 1999, Phys. Rep., 316, 339
Kramida A., Ralchenko Yu., Reader J. NIST ASD Team, 2018, NIST Atomic Spectra Database (ver. 5.5.6), Online, National Institute of Standards and Technology, Gaithersburg, MD, Available: https://physics.nist.gov/asd, 2018, July 25
Liang G. Y., Whiteford A. D., Badnell N. R., 2009, J. Phys. B: At. Mol. Opt. Phys., 42, 225002
Ludlow J. A., Ballance C. P., Loch S. D., Pindzola F. S., 2010, J. Phys. B: At. Mol. Opt. Phys., 43, 074029
Mohan M., Le Dourneuf M., Hibbert A., 1991, J. Phys. B: At. Mol. Opt. Phys., 24, 299
Munoz Burgos J. M., Ballance C. P., Loch S. D., Boivin R. F., 2009, A&A, 500, 1253
Natarajan L., Mulye Y. G., 2001, J. Phys. B: At. Mol. Opt. Phys., 34, 1839
Rauch T., Ziegler M., Werner K., Kruk J. W., Oliveira C. M., Vande Putte D., Mignani R. P., Kerber F., 2007, A&A, 470, 317
Saraph H., 1978, Comput. Phys. Comm., 15, 274
Werner K., Rauch T., Kruk J. W., 2007, A&A, 446, 317
Werner K., Rauch T., Kruk J. W., 2017, A&A, 601, A8
Wesemael F., 1981, ApJS, 45, 177
Zhou C., Cao J-J., Liang L., Yu G-H., Wang Z-M., He H-Y., 2015, Optik, 126, 4105

This paper has been typeset from a TEX/LATEX file prepared by the author.